Enhanced gamma-ray shielding and thermal-physical properties in novel zinc yttrium borate glasses

Yu. S. Hordieiev*, A. V. Zaichuk
Ukrainian State University of Science and Technologies, 8 Nauka Ave., Dnipro, 49005, Ukraine

Novel zinc yttrium borate glasses with the composition $45ZnO–(55-m)B_2O_3–mY_2O_3$ (m = 0–15 mol%) have been synthesized by melt quenching at 1350°C followed by annealing. Structural investigations confirmed complete amorphousness and progressive borate network modification from trigonal BO_3 to tetrahedral BO_4 units with increasing Y_2O_3 content. Progressive incorporation of Y_2O_3 markedly increased density (3.121–3.920 g/cm³), elevated glass transition (585–596°C) temperatures, and significantly enhanced crystallization resistance. Radiation shielding analysis revealed a significant enhancement in linear attenuation coefficient (from 7.29 to 18.67 cm^{-1} at 0.0395 MeV) and effective atomic number (from 25.01 to 32.48), accompanied by a 61% reduction in the tenth-value layer. These trends, consistent across gamma energies up to 1.458 MeV, confirm that substituting B_2O_3 with Y_2O_3 enhances both structural stability and shielding efficiency, positioning ZBY glasses as strong candidates for advanced radiation protection applications.

(Received May 15, 2025; Accepted August 1, 2025)

Keywords: Borate glasses, Differential thermal analysis, Density, Gamma-ray shielding, Thermal expansion

1. Introduction

Borate glasses form a unique class of amorphous materials characterized by a flexible network structure and outstanding thermal and optical properties [1]. In vitreous B_2O_3, boron atoms primarily coordinate with oxygen in trigonal planar BO_3 units, but can convert to tetrahedral BO_4 units upon the incorporation of modifiers, allowing a flexible network structure. This structural adaptability enables borate glasses to accommodate various additive oxides and achieve a broad range of properties. Notably, heavy metal and rare-earth doped borate glasses have attracted great interest as advanced optical and shielding materials. They offer the advantages of high density, high refractive index, and transparency while being processed at relatively low melting temperatures [2, 3]. These attributes make heavy-metal borate glasses promising for radiological applications: for example, bismuth borate compositions are reported [4, 5] to be non-toxic, lead-free alternatives with superior gamma-ray attenuation and visible light transparency. Similarly, rare-earth (RE) containing borate glasses exhibit enhanced attenuation of ionizing radiation due to the increased effective atomic number and density conferred by the RE ions [6, 7]. Such features underline the significance of borate glass networks as adaptable hosts for developing new radiation-shielding materials.

The addition of ZnO is known to significantly modify the structure and stability of borate glasses. Zinc oxide acts as an intermediate oxide in the borate network, capable of converting some trigonal BO_3 units into BO_4 tetrahedra and thus increasing the network connectivity [8]. The heavier Zn^{2+} ions (atomic mass 65.4), which replace B^{3+} (atomic mass 10.8), result in a higher glass density and a decrease in molar volume with increasing zinc oxide content [9]. Importantly, ZnO additions enhance the thermal stability of borate glasses by suppressing crystallization, and they improve the chemical durability of the glass matrix [10, 11]. These known benefits – denser, more durable networks with greater resistance to devitrification – make ZnO-containing borate glasses more robust for practical use, and this composition is often associated with improved mechanical strength and the ability to accommodate functional dopants for optical or electronic applications [12].

* Corresponding author: yuriihordieiev@gmail.com
https://doi.org/10.15251/DJNB.2025.203.901

Rare-earth oxides like yttrium oxide (Y_2O_3) further expand the performance envelope of borate glass systems. Y_2O_3 is an intermediate oxide that integrates into the borate network, yielding glasses with superior chemical durability and mechanical strength [13, 14]. Experiments show that introducing even a few mole-percent of Y_2O_3 can dramatically reduce aqueous leaching (i.e., improve durability) and more than double the Vickers hardness in related borate networks [14, 15]. Yttrium's high-field-strength cation (Y^{3+}) strengthens the glass structure, and its presence contributes to a higher overall density and thermal stability in the glass [16]. Moreover, rare-earth-doped glasses exhibit enhanced resistance to radiation: the addition of Y_2O_3 or similar lanthanide oxides increases the effective atomic number of the glass, improving its ability to attenuate ionizing radiation [17, 18]. In essence, Y_2O_3 imparts a combination of chemical robustness, mechanical rigidity, and radiation tolerance to borate glasses, making such rare-earth-modified glasses highly desirable for demanding environments.

In light of the above, the present study aims to synthesize and characterize a novel series of zinc yttrium borate glasses with the nominal formula $45ZnO–(55–m)B_2O_3–mY_2O_3$, where m varies from 0 to 15 mol%. By systematically substituting Y_2O_3 for B_2O_3 in the glass (while keeping ZnO constant at 45 mol%), we investigate how increasing Y_2O_3 content influences the glasses' structural arrangement, thermal properties, and radiation shielding behavior. Particular emphasis is placed on evaluating gamma-ray attenuation with an Eu-152 source, to understand the shielding efficacy of these glasses at diagnostic and intermediate gamma energies. The ultimate goal is to identify composition–property relationships that could guide the development of lead-free, radiation-resistant glass materials for use in diagnostic radiology, nuclear technology, and radiation protection.

2. Materials and methods

A series of novel zinc yttrium borate (ZBY) glasses was fabricated with the general chemical composition $45ZnO–(55-m)B_2O_3–mY_2O_3$, where m denotes the progressive substitution of boron oxide (B_2O_3) by yttrium oxide (Y_2O_3) in incremental steps of 0, 3, 6, 9, 12, and 15 mol%. High-purity precursors, specifically zinc oxide (≥ 99%, Reachim), boric acid (≥ 99.5%, Etimaden), and yttrium trioxide (≥ 99.99%, Sigma-Aldrich), were carefully weighed to the required compositions and thoroughly homogenized. The homogenized batch mixtures were then transferred to standard corundum crucibles and melted at 1350°C for 1 hour in a silicon carbide rod-heated furnace (Nabertherm) to achieve complete melting and homogeneity. The molten ZBY glass was poured into preheated molds to form specimens in the form of 5×5×50 mm³ rods and 30 mm diameter discs. Post-casting, the samples were annealed at 590 and 610°C temperatures in a SNOL muffle furnace for five hours to relieve internal stresses. Cooling to ambient temperature was carried out at a precisely controlled rate of 40°C per hour. Based on their yttrium trioxide content, the resulting glass samples were labeled: ZBY0 ($45ZnO–55B_2O_3$); ZBY3 ($45ZnO–52B_2O_3–3Y_2O_3$); ZBY6 ($45ZnO–49B_2O_3–6Y_2O)_3$; ZBY9 ($45ZnO–46B_2O_3–9Y_2O_3$); ZBY12 ($45ZnO–43B_2O_3–12Y_2O_3$); ZBY15 ($45ZnO–40B_2O_3–15Y_2O_3$).

Thermal characterization of the fabricated glasses was conducted using a simultaneous thermogravimetric analyzer (Nexta STA300, Hitachi, Japan) at precisely measured rates of 10°C/min to determine the $T_{g.t.}$, T_p, and T_m via DTA curve [19]. Complementary dilatometric measurements were conducted on a GT-1000 dilatometer at a precisely measured rate of 3°C/min [19] to obtain the dilatometric $T_{g.t.}$, softening point (T_{dil}), and linear thermal expansion coefficient (CTE).

Structural features were characterized by XRD (DRON-3M) and FTIR spectroscopy (IRSpirit-X, 1600-400 cm^{-1}, 4 cm^{-1} resolution, 30 scans per measurement). Samples for FTIR analysis were prepared via the potassium bromide (KBr, Specac) pellet method, with pure KBr pellets serving as background reference. Density was determined via Archimedes' technique in decane ($\rho = 0.732$ g/cm³) using a Radwag AS balance (±0.1 μg).

Radiation shielding properties of the fabricated ZBY glasses were evaluated theoretically using the Phy-X software tool [20], which is widely recognized for its accuracy in photon-material interaction modeling. The evaluation encompassed gamma-ray energies from 0.0359 to 1.46 MeV, corresponding to emissions of the widely used Eu-152 radioactive source in radiological diagnostics

and research. Parameters such as linear attenuation coefficient (LAC), tenth-value layer (TVL), and effective atomic number (Z_{eff}) were systematically calculated, thus providing detailed insights into how increased Y_2O_3 content affects radiation attenuation performance, guiding potential applications in medical imaging, nuclear research, industrial radiography, and protective systems.

3. Results and discussion

Figure 1 displays the X-ray diffraction patterns for the synthesized zinc yttrium borate (ZBY) glass series with varying Y_2O_3 content. The diffraction patterns reveal characteristic amorphous features across all compositions (ZBY0 through ZBY15), evidenced by the presence of broad humps centered around 30–33° 2-theta and the notable absence of sharp crystalline peaks. This confirms the successful formation of fully amorphous structures throughout the entire compositional range from 0 to 15 mol% Y_2O_3. Notably, with increasing Y_2O_3 content from 0 to 15 mol%, the position and shape of the primary diffraction maximum remain largely consistent, suggesting that the progressive substitution of B_2O_3 by Y_2O_3 does not fundamentally alter the short-range structural arrangement of the glass network. However, subtle variations in the intensity and full width at half maximum of the primary hump can be observed, particularly in samples with higher Y_2O_3 concentrations (ZBY9, ZBY12, and ZBY15). These minor changes indicate that while the overall amorphous character is preserved, the incorporation of Y_2O_3 likely influences the distribution of interatomic distances and potentially modifies the coordination environment of network-forming and network-modifying cations within the glass matrix.

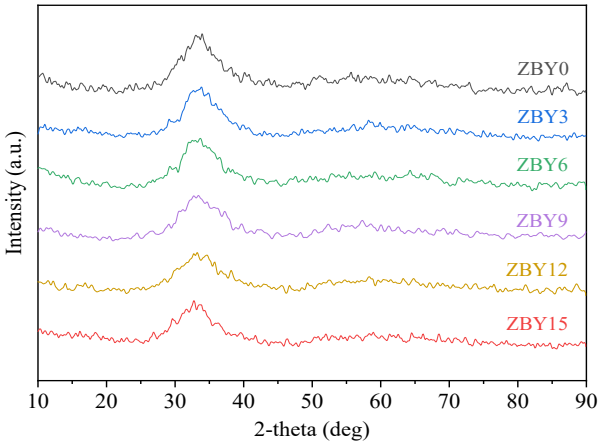

Fig. 1. XRD patterns of 45ZnO–(55-m)B_2O_3–mY_2O_3 glass samples with varying Y_2O_3 content.

Figure 2 presents the FTIR spectra of the ZBY glass series containing varying concentrations of yttrium oxide. The broad absorption bands observed are characteristic of amorphous borate-based glasses and provide insight into the structural evolution of the glass network. In the high-wavenumber region (1200–1500 cm^{-1}), bands centered at 1380 and 1256 cm^{-1} in ZBY0 correspond to asymmetric B–O stretching vibrations in trigonal BO_3 units, including metaborate and pyroborate groups [21, 22]. As Y_2O_3 content increases, these bands shift to lower wavenumbers (e.g., 1328 and 1206 cm^{-1} in ZBY15), and their intensity diminishes – indicative of a reduced concentration of BO_3 units due to their conversion to tetrahedral BO_4 units. Concurrently, the band near 1086–1022 cm^{-1}, attributed to symmetric B–O stretching in BO_4 units [23, 24], becomes more prominent, particularly in Y_2O_3-rich glasses. This transition from BO_3 to BO_4 is facilitated by the introduction of Y^{3+} ions, which, as high-field-strength modifiers, disrupt the borate network by introducing non-bridging oxygens (NBOs). The distinct band near 856 cm^{-1} observed in the FTIR spectrum of ZBY0 is characteristic of symmetric B–O–B stretching vibrations in

pyroborate (B_2O_5) dimer units [25]. The decreasing intensity of this band with increasing Y_2O_3 content suggests a gradual depolymerization or transformation of these dimeric units, likely due to the modifier action of Y^{3+} and the accompanying formation of NBOs. Meanwhile, the broad feature centered at ~686 cm^{-1} in ZBY0 gradually shifts to ~700 cm^{-1} in ZBY15. This band is associated with the bending vibrations of B–O–B bridges [26, 27], and the observed shift toward higher frequencies signifies changes in the structural and bonding environment of these linkages. Specifically, the progressive incorporation of Y^{3+} ions depolymerizes the borate network by replacing bridging oxygens with non-bridging oxygens and forming new Y–O–B bonds. In the lower wavenumber region, the emergence and intensification of bands at ~516, 464, and 424 cm^{-1} provide further evidence of structural modification. The band at ~516 cm^{-1} becomes prominent in Y_2O_3-containing samples and is attributed to Y–O stretching vibrations [28], indicating the successful incorporation of Y^{3+} ions into the glass network. The persistent band at 464 cm^{-1} is assigned to bending Zn–O vibrations within distorted ZnO_4 tetrahedra [23, 24]. Its nearly constant intensity across the series indicates that the local structural environment of Zn^{2+} ions remains largely unaffected by Y_2O_3 incorporation, suggesting that the zinc-oxygen coordination framework is structurally stable despite progressive modifications to the borate network. The lowest frequency band at ~424 cm^{-1} is tentatively attributed to vibrational modes involving Zn^{2+} cations in various coordination environments [9].

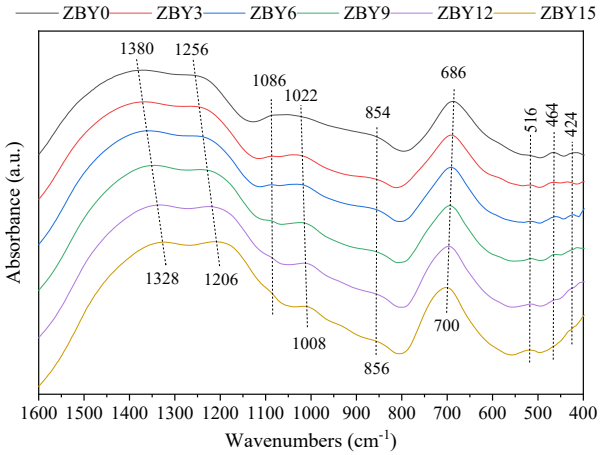

Fig. 2. Infrared spectra of ZBY glasses showing vibrational changes with increasing Y_2O_3 content.

The physical properties of the ZBY glass series exhibit a strong dependence on Y_2O_3 content, as illustrated in Figure 3. The density and molar volume of the glasses systematically increase with the progressive substitution of B_2O_3 by Y_2O_3.

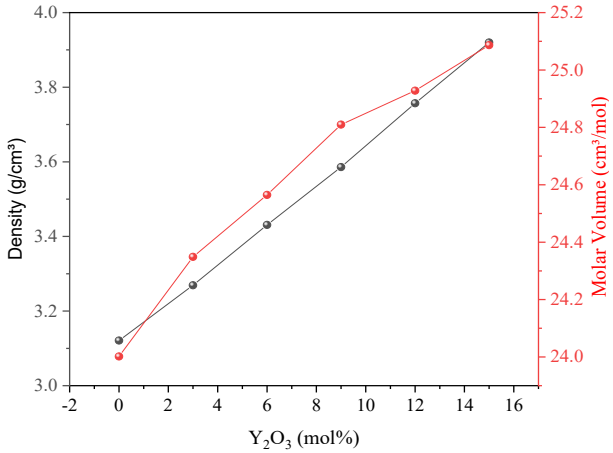

Fig. 3. Effect of Y_2O_3 substitution on the density and molar volume of $45ZnO–(55-m)B_2O_3–mY_2O_3$ glasses.

The density (represented by black circles) shows a nearly linear progression from 3.121 g/cm³ for the base ZBY0 composition (45ZnO–55B_2O_3) to 3.920 g/cm³ for ZBY15 (45ZnO–40B_2O_3–15Y_2O_3), representing a substantial increase of approximately 25.6%. This pronounced densification effect can be primarily attributed to the significantly higher atomic weight of Y_2O_3 (225.81 g/mol) compared to B_2O_3 (69.62 g/mol). Concurrently, the molar volume (shown by red circles) also increases consistently from 24.002 cm³/mol for ZBY0 to 25.087 cm³/mol for ZBY15, although this increase (approximately 4.5%) is less dramatic than that observed for density. This simultaneous increase in both density and molar volume is noteworthy, as it diverges from the inverse relationship often observed in many glass systems [29]. The parallel increase suggests that while Y_2O_3 incorporation substantially increases the overall mass of the glass network, it also induces structural expansion. This expansion can be attributed to the larger ionic radius of Y^{3+} (0.9 Å) compared to B^{3+} (0.1–0.2 Å, depending on coordination) [30], which necessitates greater interatomic spacing within the glass network. The increase in molar volume also aligns with the FTIR observations regarding network depolymerization, as the disruption of the rigid borate network by Y^{3+} ions creates a more open and less tightly connected glass structure. These physical property trends have significant implications for the radiation shielding capabilities of these glasses, as higher-density materials generally exhibit enhanced gamma-ray attenuation performance.

The thermal behavior of the ZBY glass series demonstrates a systematic dependence on Y_2O_3 concentration, as evidenced by the DTA curves presented in Figure 4.

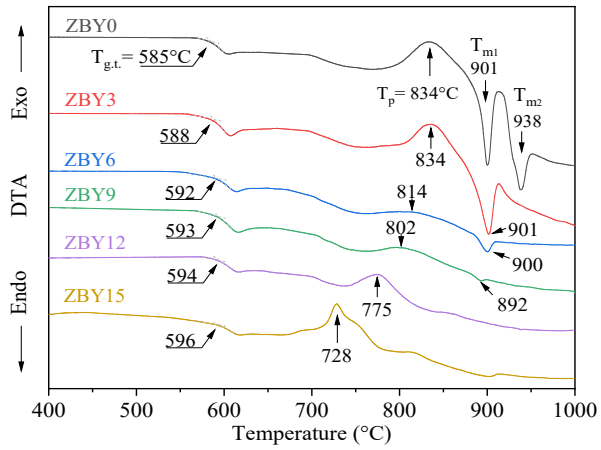

Fig. 4. DTA thermograms of ZBY glasses with varying Y_2O_3 content.

All compositions display characteristic thermal events: a glass transition indicated by endothermic deflection ($T_{g.t.}$), an exothermic crystallization peak (T_p), and endothermic melting events (T_m). The $T_{g.t.}$ values show a modest but consistent increase with Y_2O_3 content, rising from 585°C for the base ZBY0 composition to 596°C for ZBY15, representing an increment of approximately 11°C. This trend indicates enhanced network rigidity and glass stability at the atomic scale, which can be attributed to the network stabilization caused by Y^{3+} ions, which act as high-field-strength cations, forming additional cross-linking Y–O–B bonds and restricting the mobility of the glass structure, despite Y–O bonds being weaker than B–O bonds. Conversely, the peak crystallization temperature (T_p) systematically decreases from 834 °C (ZBY0) to 728 °C (ZBY15), reflecting the network-modifying role of Y^{3+} ions and the introduction of NBOs, which promote localized structural rearrangement. Notably, the intensity of the crystallization exotherms progressively diminishes as Y_2O_3 content increases. In particular, ZBY0 displays a sharp and pronounced exothermic peak at 834 °C, reflecting a high tendency toward crystallization. In contrast, the exothermic peaks in ZBY6 and ZBY9 are considerably weaker and broader, indicating that the glasses become increasingly resistant to crystallization with higher Y_2O_3 content. This

significant decrease in crystallization peak intensity suggests a reduced tendency for devitrification and an enhancement in glass stability with increasing Y_2O_3 content.

The crystallization behavior and phase evolution upon controlled heat treatment are further elucidated in Figure 5, which presents the XRD patterns of selected compositions after isothermal crystallization at their respective peak crystallization temperatures for 5 hours. For ZBY0, a complex diffraction pattern emerges, with well-defined peaks corresponding to the crystalline phases $Zn_4B_6O_{13}$ (Ref. code 01–076–0917) and $Zn_4B_2O_7$ (Ref. code 01–085–1778), indicating substantial crystallization of zinc borates. However, as the Y_2O_3 content increases, the crystallization behavior markedly shifts. In the ZBY12 and ZBY15 samples, the dominant crystalline phases are YBO_3 (Ref. code 01–083–1205) and ZnO_2 (Ref. code 00–001–1150), with the absence of zinc borate phases observed in ZBY0. This transition underscores the strong influence of Y_2O_3 on modifying the glass network and the resulting crystallization pathways. The appearance of YBO_3 confirms that Y^{3+} ions not only act as network modifiers but also participate in the formation of new yttrium-containing crystalline phases during heat treatment. Furthermore, the reduction in the number and intensity of diffraction peaks in Y_2O_3-rich samples suggests a lower degree of overall crystallinity, consistent with the DTA findings of broader and weaker crystallization exotherms.

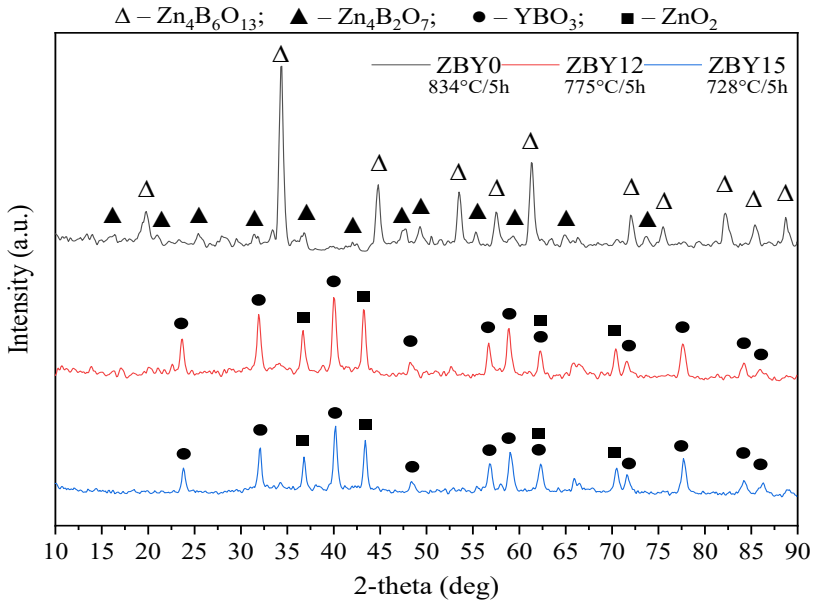

Fig. 5. XRD patterns of heat-treated ZBY0, ZBY12, and ZBY15 glasses after 5-hour crystallization.

The influence of Y_2O_3 content on the thermal expansion behavior of the ZBY glass series is comprehensively illustrated in Figure 6. The dilatometric curve, exemplified by glass sample ZBY0 (Fig. 6, left), clearly depicts typical glassy behavior, where the linear dimension ($\Delta L/L$) initially increases gradually with temperature until a significant slope change occurs at the glass transition region ($T_{g.t.}$). Following $T_{g.t.}$, a pronounced increase in expansion is observed, continuing up to the dilatometric softening point (T_{dil}), marking the onset of viscous flow. Specifically, for the ZBY0 composition, the dilatometric CTE value measured from the linear region before the glass transition is 4.67 ppm/°C, with the $T_{g.t.}$ and T_{dil} identified as 587°C and 612°C, respectively. The right panel of Figure 6 provides a comprehensive view of how the thermal parameters – CTE, $T_{g.t.}$, and T_{dil} – evolve across the compositional series with increasing Y_2O_3 substitution from 0 to 15 mol%. A consistent increase in $T_{g.t.}$ from 587°C (ZBY0) to 600°C (ZBY15) and T_{dil} from 612°C (ZBY0) to 629°C (ZBY15) is observed. The gradual elevation in both temperatures aligns closely with previous DTA analyses, underscoring enhanced network rigidity and structural stability imparted by Y_2O_3 substitution. Concurrently, the CTE increases markedly from 4.67 ppm/°C in ZBY0 to 6.24 ppm/°C in ZBY15. The notable rise in thermal expansion coefficients with increased Y_2O_3 content is

consistent with the structural transformations indicated by FTIR spectroscopy, particularly the depolymerization of the borate network and formation of NBOs. These structural modifications facilitate increased structural openness and flexibility, thus promoting greater thermal expansion. Consequently, while the incorporation of Y_2O_3 strengthens the glass network thermally, it also contributes to structural rearrangements that result in higher thermal expansivity, crucial for tailoring these glasses toward specific technological applications, such as precision sealing materials or components subject to controlled thermal expansion demands.

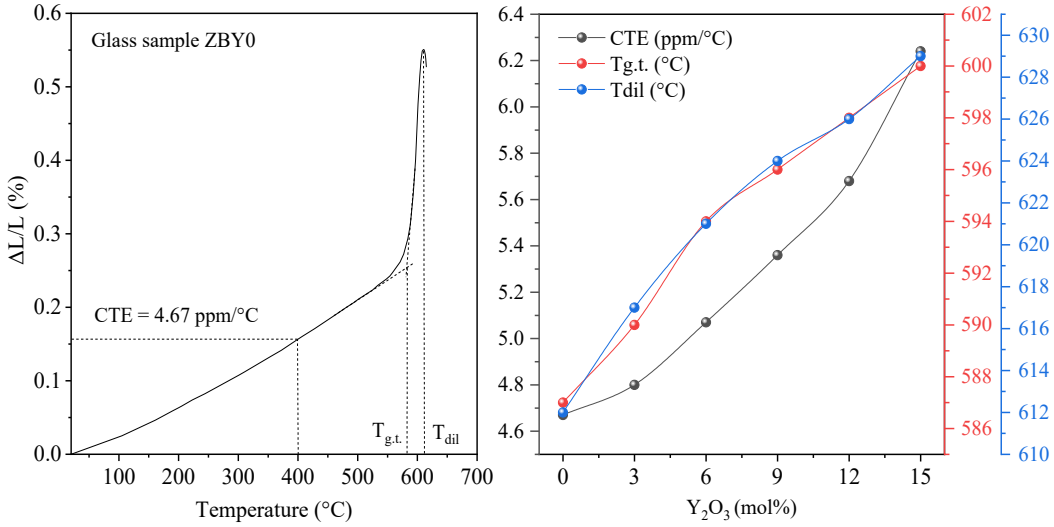

Fig. 6. Dilatometric thermal behavior and expansion characteristics of ZBY glasses.

Figure 7 illustrates the energy-dependent behavior of the linear attenuation coefficient (LAC) for the synthesized zinc yttrium borate glass series across a gamma-ray energy range of 0.0395 to 1.458 MeV, corresponding to typical energies emitted by an Eu-152 radioactive source commonly employed in diagnostic radiology and nuclear research. The LAC values exhibit a characteristic exponential decay with increasing photon energy, demonstrating the typical attenuation behavior of materials against gamma radiation. In the low-energy regime (< 0.1 MeV), where photoelectric absorption dominates the interaction mechanism, LAC values are significantly higher, ranging from 7.29 cm^{-1} for ZBY0 to 18.67 cm^{-1} for ZBY15 at 0.0395 MeV. This represents a remarkable enhancement of approximately 156% in attenuation capability with the maximum Y_2O_3 substitution.

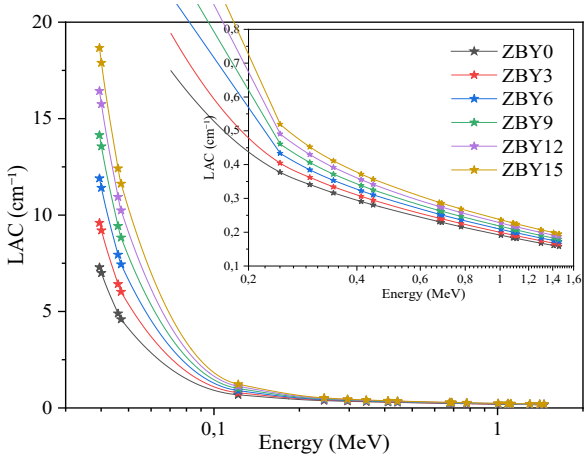

Fig. 7. Energy-dependent LAC for ZBY glass series with varying Y_2O_3 content.

At higher energies (above 0.2 MeV), the attenuation values converge closer together, as is typical for high-energy photons where Compton scattering dominates. Nevertheless, even at energies up to 1.458 MeV, a discernible improvement in radiation shielding efficiency is maintained in compositions richer in Y_2O_3. For example, at 1.458 MeV, the LAC for ZBY15 remains higher (0.19531 cm^{-1}) compared to ZBY0 (0.15784 cm^{-1}). The inset of Figure 7 further emphasizes this trend, providing a clearer visualization of the LAC behavior at intermediate photon energies (0.2 to 1.6 MeV), and confirming the consistent enhancement in attenuation properties with increasing Y_2O_3 content across the entire energy spectrum evaluated.

The systematic improvement in LAC with increasing Y_2O_3 content correlates with the density enhancement observed in Figure 3, confirming that the combined effects of higher atomic mass and increased material density contribute synergistically to enhanced photon attenuation. These results indicate that the substitution of B_2O_3 with Y_2O_3 not only modifies the glass structure as evidenced by FTIR analysis but also significantly improves radiation shielding capabilities, making these glasses particularly suitable for applications requiring both structural integrity and radiation protection [9].

Figure 8 illustrates the variation of the tenth-value layer (TVL), a crucial parameter representing the thickness required to reduce gamma radiation intensity to one-tenth of its initial value, across the energy range of 0.0395 to 1.458 MeV for ZBY glass samples with varying Y_2O_3 concentrations. The trends clearly demonstrate a pronounced influence of yttrium oxide content on the radiation shielding [31] capabilities of these glasses.

As clearly seen in Figure 8, the TVL values for all ZBY compositions increase progressively with photon energy, a direct consequence of the decreasing linear attenuation coefficient (LAC) observed in Figure 7. Importantly, at all energies evaluated, glasses with higher Y_2O_3 content exhibit consistently lower TVL values, reflecting superior radiation attenuation performance due to their increased density and effective atomic number [32]. For example, at the lower energy limit (0.0395 MeV), the TVL decreases significantly from 0.31573 cm for ZBY0 (no yttrium) to 0.12335 cm for ZBY15 (15 mol% Y_2O_3), representing a reduction of approximately 61%. Such substantial enhancement underscores the profound influence of Y_2O_3 incorporation on shielding efficiency, particularly at lower photon energies dominated by the photoelectric effect [19].

At higher energies (e.g., 1.458 MeV), although the absolute TVL values are inherently greater, a clear advantage of Y_2O_3-containing glasses remains evident. Here, the TVL decreases from 14.58795 cm (ZBY0) to 11.78963 cm (ZBY15), indicating an approximate 19% improvement in shielding effectiveness. This trend highlights the capability of yttrium oxide to enhance gamma-ray shielding even within the higher-energy regime predominantly governed by Compton scattering interactions.

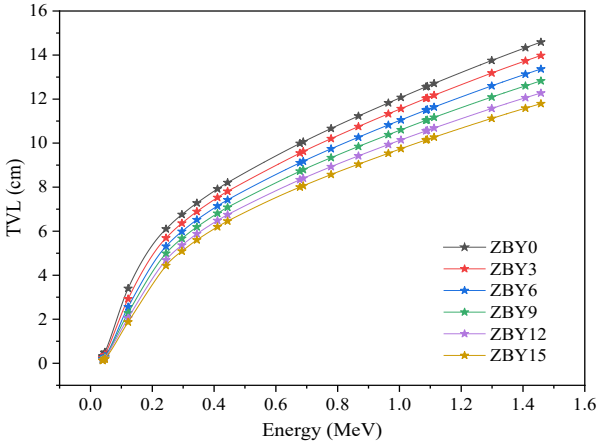

Fig. 8. TVL of ZBY glasses as a function of γ-ray energy for varying Y_2O_3 content.

Figure 9 provides detailed insights into how the effective atomic number (Z_{eff}), an important parameter for the radiation shield efficiency, varies across the gamma-ray energy spectrum (0.0395 to 1.458 MeV) for the synthesized zinc yttrium borate glasses. The effective atomic number, a critical parameter in radiation physics that characterizes a material's radiation interaction properties, demonstrates pronounced variation both with incident photon energy and Y_2O_3 concentration in the borate glass matrix.

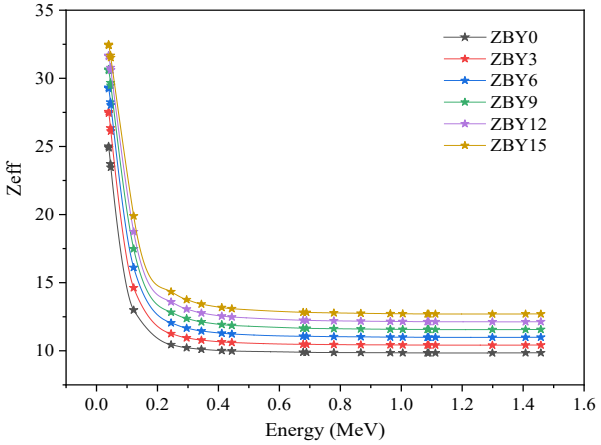

Fig. 9. Z_{eff} of ZBY glasses as a function of γ-ray energy for varying Y_2O_3 content.

The impact of incorporating yttrium oxide into the glass network is clearly observable. Specifically, Z_{eff} values consistently increase with the Y_2O_3 content across all energies measured, indicating enhanced photon interaction capabilities and, thus, superior shielding performance. At the lowest recorded energy of 0.0395 MeV, Z_{eff} rises markedly from 25.01 in ZBY0 (no yttrium) to 32.48 in ZBY15 (15 mol% Y_2O_3), highlighting an improvement of approximately 30%. This significant improvement in Z_{eff} directly correlates with the superior radiation attenuation capabilities observed at low energies and supports the LAC findings presented in Figure 7.

At intermediate photon energies (e.g., 0.1218 MeV), the variation in Z_{eff} among different compositions remains clearly distinguishable, albeit less pronounced compared to lower energies. For instance, Z_{eff} increases progressively from 12.99 (ZBY0) to 19.89 (ZBY15), confirming the sustained effectiveness of yttrium substitution in enhancing radiation shielding capabilities even at these intermediate energies. At higher energies (above approximately 0.4 MeV), Z_{eff} values become relatively constant, exhibiting only slight increases with greater yttrium content. For instance, at 1.458 MeV, Z_{eff} ranges narrowly from 9.85 (ZBY0) to 12.70 (ZBY15), indicating a limited but consistent advantage for glasses containing higher Y_2O_3 concentrations. This observation can be attributed to the fact that Compton scattering, being less dependent on atomic number, becomes the dominant photon interaction mechanism in this region.

Z_{eff}'s energy-dependent behavior complements the previously discussed LAC and TVL trends, providing a more comprehensive understanding of the radiation interaction mechanisms in these glasses. The consistently higher Z_{eff} values observed in Y_2O_3-rich compositions across all energies confirm their superior radiation attenuation capabilities, particularly at diagnostic imaging energies (<0.1 MeV). This enhancement can be attributed to the significantly higher atomic number of yttrium (Z=39) compared to boron (Z=5), which facilitates more efficient photoelectric absorption.

Overall, the trends observed in Figure 9 reveal that the incremental replacement of B_2O_3 with Y_2O_3 not only increases the density of the glasses, as noted earlier, but also significantly enhances their effective atomic number, significantly enhancing radiation shielding performance across a broad energy range. These findings clearly support the potential application of yttrium-rich zinc borate glasses as efficient gamma-ray shielding materials in medical, industrial, and nuclear safety contexts.

4. Conclusions

A series of novel zinc yttrium borate glasses with the composition $45ZnO–(55-m)B_2O_3–mY_2O_3$ (m = 0–15 mol%) was successfully synthesized and comprehensively characterized. The progressive substitution of B_2O_3 by Y_2O_3 induced significant structural modifications, as evidenced by FTIR spectroscopy, including the conversion of trigonal BO_3 to tetrahedral BO_4 units and network depolymerization through the formation of NBOs. These structural changes correlated with a substantial density increase from 3.121 g/cm³ (ZBY0) to 3.920 g/cm³ (ZBY15, representing a 25.6% rise), and a simultaneous molar volume increment from 24.002 to 25.087 cm³/mol. Thermal analysis revealed that glass transition ($T_{g.t.}$) and softening point (T_{dil}) increased modestly from 585 to 596°C and 612 to 629°C, respectively, suggesting enhanced structural rigidity. Notably, the peak crystallization temperature reduced from 834°C (ZBY0) to 728°C (ZBY15), with Y_2O_3-rich compositions exhibiting reduced crystallization tendency and altered crystallization pathways, transitioning from zinc borate phases ($Zn_4B_6O_{13}$, $Zn_4B_2O_7$) in ZBY0 to predominantly YBO_3 in Y_2O_3-containing glasses.

The radiation shielding properties of the ZBY glasses were significantly enhanced with increasing Y_2O_3 content across the evaluated gamma-ray energy range (0.0395–1.458 MeV). At 0.0395 MeV, the LAC dramatically increased from 7.29 cm^{-1} (ZBY0) to 18.67 cm^{-1} (ZBY15), a 156% enhancement. Correspondingly, the TVL decreased significantly by approximately 61%, from 0.31573 cm (ZBY0) to 0.12335 cm (ZBY15). Similarly, the effective atomic number increased from 25.01 to 32.48 at this energy, confirming superior photoelectric absorption. Even at higher energies dominated by Compton scattering, Y_2O_3-rich compositions maintained improved shielding efficiency, with approximately 19% lower TVL values at 1.458 MeV (from 14.58795 to 11.78963 cm). This systematic enhancement positions Y_2O_3-rich zinc borate glasses as promising materials for radiation shielding in medical diagnostics, nuclear safety, and industrial radiography, thus extending the applicability and performance of borate-based glass systems.

References

[1] M. Bengisu, Journal of Materials Science **51**, 2199 (2016); https://doi.org/10.1007/s10853-015-9537-4
[2] Yu. S. Hordieiev, A. V. Zaichuk, Digest Journal of Nanomaterials and Biostructures **19**, 773 (2024); https://doi.org/10.15251/DJNB.2024.192.773
[3] B. V. Padlyak, I. I. Kindrat, Y. O. Kulyk, S. I. Mudry, A. Drzewiecki, Y. S. Hordieiev, V. I. Goleus, R. Lisiecki, Mater. Sci. Eng. B Solid State Mater. Adv. Technol. **278**, 115655 (2022); https://doi.org/10.1016/j.mseb.2022.115655
[4] Y. S. Rammah, M. I. Sayyed, A. A. Ali, H. O. Tekin, R. El-Mallawany, Appl. Phys. A **124**, 832 (2018); https://doi.org/10.1007/s00339-018-2252-7
[5] M. I. Sayyed, M. H. A. Mhareb, Y. S. M. Alajerami, K. A. Mahmoud, M. A. Imheidat, F. Alshahri, M. Alqahtani, T. Al-Abdullah, Optik **239**, 166790 (2021); https://doi.org/10.1016/j.ijleo.2021.166790
[6] M. K. Hossain, G. A. Raihan, M. A. Akbar, M. H. Kabir Rubel, M. H. Ahmed, M. I. Khan, S. Hossain, S. K. Sen, M. I. E. Jalal, A. El-Denglawey, ACS Appl. Electron. Mater. **4**, 3327 (2022); https://doi.org/10.1021/acsaelm.2c00069
[7] Z. A. Alrowaili, T. A. Taha, M. Ibrahim, K. M. A. Saron, Eur. Phys. J. Plus **136**, 567 (2021); https://doi.org/10.1140/epjp/s13360-021-01565-y
[8] Y. S. Hordieiev, A. V. Zaichuk, MRS Advances **8**, 201 (2023); https://doi.org/10.1557/s43580-023-00511-7
[9] Y. Hordieiev, A. Zaichuk, Sci. Rep. **15**, 16158 (2025); https://doi.org/10.1038/s41598-025-96015-5
[10] G. Della Mea, A. Gasparotto, M. Bettinelli, A. Montenero, R. Scaglioni, J. Non Cryst. Solids **84**, 443 (1986); https://doi.org/10.1016/0022-3093(86)90808-2
[11] V. I. Goleus, Y. S. Hordieiev, A. V. Nosenko, Voprosy Khimii i Khimicheskoi Tekhnologii **4**, 92 (2018).

[12] H. M. Gomaa, I. S. Yahia, B. M. A. Makram, A. H. El-Dosokey, S. M. Elkatlawy, J Mater Sci: Mater Electron **32**, 9392 (2021); https://doi.org/10.1007/s10854-021-05602-5
[13] Q. M. Saleem, H. A. Abo-Mosallam, E. A. Mahdy, K.A. Aly, M. M. Ebrahium, Ceram. Int. **55**(9), 11097 (2025); https://doi.org/10.1016/j.ceramint.2024.12.528
[14] M. Wang, A. Li, X. Zhang, D. Zhang, S. Jin, D. Xiong, W. Deng, J. Rare Earths **40**, 1316 (2022); https://doi.org/10.1016/j.jre.2021.08.010
[15] H. A. Thabit, A. K. Ismail, M. H. A. Mhareb, D. A. Abdulmalik, Abdullahi I, A. M. Al-Fakih, Y. S. M. Alajerami, S. Hashim, Heliyon **9**, e18309 (2023); https://doi.org/10.1016/j.heliyon.2023.e18309
[16] Yu. S. Hordieiev, A. V. Zaichuk, Journal of Inorganic and Organometallic Polymers and Materials **33**(2), 591 (2023); https://doi.org/10.1007/s10904-022-02526-3
[17] E. M. Ahmed, A. A. Elzelaky, N. A. El-Ghamaz, M. I. Youssif, Radiat. Phys. Chem. **216**, 111457 (2024); https://doi.org/10.1016/j.radphyschem.2023.111457
[18] M. I. Sayyed, M. H. A. Mhareb, R. I. Mahdi, A. J. Kadhim, K. M. Kaky, M. K. Hamad, Ceram. Int. **50**, 54490 (2024); https://doi.org/10.1016/j.ceramint.2024.10.305
[19] Y. S. Hordieiev, A. V. Zaichuk, J. Ovonic Res. **21**, 85 (2025); https://doi.org/10.15251/jor.2025.211.85
[20] E. Şakar, Ö. F. Özpolat, B. Alım, M. I. Sayyed, M. Kurudirek, Radiation Physics and Chemistry **166**, 108496 (2020); https://doi.org/10.1016/j.radphyschem.2019.108496
[21] L. M. Osipova, A. A. Osipov, A. A. Osipov, Glass Phys Chem **45**, 182 (2019); https://doi.org/10.1134/S1087659619030076
[22] R. Iordanova, M. Milanova, A. Yordanova, L. Aleksandrov, N. Nedyalkov, R. Kukeva, P. Petrova, Materials **17**, 1415 (2024); https://doi.org/10.3390/ma17061415
[23] J. Ahlawat, S. Pawaria, N. Deopa, S. Dahiya, R. Punia, A.S. Maan, Appl. Phys. A **128**, 923 (2022); https://doi.org/10.1007/s00339-022-05997-w
[24] K. Hanamar, B. G. Hegde, S. B. Kolavekar, N. H. Ayachit, A. G. Pramod, K. Keshavamurthy, M. H. Anandalli, R. F. Bhajantri, J Inorg Organomet Polym **33**, 1612 (2023); https://doi.org/10.1007/s10904-023-02585-0
[25] B. Topper, D. Möncke, R. E. Youngman, C. Valvi, E. I. Kamitsos, C. P. E. Varsamis, Phys. Chem. Chem. Phys. **25**, 5967 (2023); https://doi.org/10.1039/d2cp05517a
[26] M. Abdel-Baki, F. El-Diasty, J. Solid State Chem. **184**, 2762 (2011); https://doi.org/10.1016/j.jssc.2011.08.015
[27] Yu. S. Hordieiev, A. V. Zaichuk, Journal of Ovonic Research **20**(3), 273 (2024); https://doi.org/10.15251/jor.2024.203.273
[28] K. S. Shaaban, A. M. Al-Baradi, Z. A. Alrowaili, A. M. Ali, M. S. Al-Buriahi, E. A. A. Wahab, J Mater Sci: Mater Electron **32**, 28065 (2021); https://doi.org/10.1007/s10854-021-07158-w
[29] D. Souri, Optothermal properties of vanadate-tellurite oxide glasses and some suggested applications, in: Tellurite Glass Smart Materials, Springer International Publishing, Cham, 67 (2018); https://doi.org/10.1007/978-3-319-76568-6_5
[30] E. J. W. Whittaker, R. Muntus, Geochim. Cosmochim. Acta **34**, 945 (1970); https://doi.org/10.1016/0016-7037(70)90077-3
[31] G. A. Alharshan, S. M. Shaaban, S. A. Said, A. M. A. Mahmoud, A. A. Altohamy, R. A. Elsad, N. M. Ebrahem, J. Inorg. Organomet. Polym. Mater. (2024); https://doi.org/10.1007/s10904-024-03461-1
[32] N. Almousa, S. A. M. Issa, H. M. H. Zakaly, D. E. Abulyazied, A. S. Abouhaswa, H. O. Tekin, Opt. Mater. **154**, 115770 (2024); https://doi.org/10.1016/j.optmat.2024.115770